in dioxane predict similar rotational populations.

Fluorescence decay measurements provide a reasonable estimate of the relative rotamer populations because other variables contributing to the preexponential factors are unaffected by rotational isomerism in this system. This information can be used to construct realistic models that may predict the dimensions and characteristics of (+)-catechin and (−)-epicatechin polymers in solution. It is clear that the existence of rotational isomerism in the dimers has profound implications for the conformations of the high polymers. This point will receive amplification elsewhere.[19,20]

Acknowledgment. This research was supported by National Science Foundation Grants DMR 86-96070 and DMR 86-96071.

Registry No. epi(4β→8)cat, 20315-25-7; epi(4β→6)cat, 12798-59-3; epi(4β→8)cat Ac, 21179-20-4; epi(4β→8)cat Br, 103883-03-0; (+)-catechin, 154-23-4; (−)-epicatechin, 490-46-0.

A Molecular Water-Oxidation Catalyst Derived from Ruthenium Diaqua Bis(2,2′-bipyridyl-5,5′-dicarboxylic acid)

Francois P. Rotzinger,[†] Shekhar Munavalli,[†1a] Pascal Comte,[†] James K. Hurst,[†1b] Michael Gratzel,* Fu-Jann Pern,[‡] and Arthur J. Frank*[‡]

Contribution from the Institut de Chimie Physique, Ecole Polytechnique Federale, CH-1015 Lausanne, Switzerland, and Solar Energy Research Institute, Golden, Colorado 80401. *Received October 6, 1986*

Abstract: Controlled-potential electrolysis of *cis*-$Ru^{II}L_2(OH_2)_2^{2+}$ (where L is 2,2′-bipyridyl-5,5′-dicarboxylic acid) in 0.5 M H_2SO_4 solutions leads to the formation of a relatively durable and active molecular water-oxidation catalyst. Detailed analyses by UV–visible absorption spectrophotometry, resonance Raman spectrophotometry, electrochemical measurements, HPLC, and elemental analysis indicate that the water-oxidation catalyst is an oxo-bridged dimer, $L_2(H_2O)Ru–O–Ru(OH_2)L_2$. The synthesis, spectrophotometric, and redox properties of the monomeric and dimeric ruthenium complexes have been characterized. The effectiveness of the oxo-bridged complex as a water-oxidation catalyst has been evaluated by electrochemical and spectrophotometric analyses and by determination of oxygen production. This newly discovered homogeneous catalyst is highly effective in mediating the thermal and visible-light-induced generation of oxygen from water. A comparison is made between the monomer and dimer and various analogues of the complexes. The presence of the COOH groups at the 5,5′ positions of the bipyridyl ligands correlates with the unusual and favorable properties of *cis*-$RuL_2(OH_2)_2$ and $L_2(OH_2)Ru–O–Ru(OH_2)L_2$. Dimeric ruthenium complexes of similar structure are also formed during the thermolysis and photolysis of Ru(II) tris-(2,2′-bipyridyl-5,5′-dicarboxylic acid), RuL_3^{2+}, in 0.5 M H_2SO_4 solutions containing peroxodisulfate.

Molecular catalysts for the oxidation of water to oxygen are under active investigation.[2-7] Of particular interest are complexes derived from transition metals such as ruthenium, since these compounds provide molecular models for processes occurring on the surface of heterogeneous water-oxidation catalysts, e.g., colloidal RuO_2.[8] Among the ruthenium complexes being investigated, oxo-bridged dimers with bipyridyl ligands are receiving increasing attention[3-7] since the discovery[9] of this class of compounds. The presence of two Ru centers with aqua ligands and multiple redox states with potentials suitable for oxygen evolution makes these complexes attractive candidates for water-oxidation catalysis.

Visible-light-induced oxygen generation has been observed[7] in dilute sulfuric acid solutions containing ruthenium(II) tris(2,2′-bipyridyl-4,4′-dicarboxylic acid) as a redox sensitizer and peroxodisulfate as an electron acceptor. Electrochemical analysis has indicated that a species capable of oxidizing water to O_2 was formed in situ from the oxidized form of the ruthenium complex. The amount of O_2 produced was, however, quite small and the O_2-evolving species was unstable. In an effort to develop a more effective water-oxidation catalyst, we have investigated the 5,5′-dicarboxylic acid derivative of $Ru(bipy)_3^{2+}$, i.e., RuL_3^{2+}, where

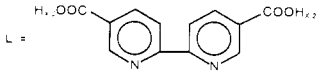

The change in the carboxylic acid groups from the 4,4′ to the 5,5′ positions of the bipyridyl ligands affects both the durability and the activity of the catalyst. Research was subsequently undertaken to identify the catalytically active species which are produced either by thermolysis or photolysis of RuL_3^{2+} in 0.5 M

[†] Ecole Polytechnique Federale.
[‡] Solar Energy Research Institute.

(1) Invited professor, on leave of absence from: (a) The Chemical Research and Development Center of the U.S. Army, Edgewood, MD; (b) the Department of Chemistry, Oregon Graduate Center, Beaverton, OR 97006.

(2) (a) Nijs, H.; Cruz, M.; Fripiat, J. J.; Van Damme, H. *J. Chem. Soc., Chem. Commun.* **1981**, 1026. (b) Nijs, H.; Cruz, M.; Fripiat, J. J.; Van Damme, H. *Nouv. J. Chim.* **1982**, *6*, 551. (c) Elizarova, G. L.; Matvienko, L. G.; Nozhkina, N. V.; Maizlish, V. E.; Parmon, V. N. *React. Kinet. Catal. Lett.* **1981**, *16*, 191. (d) Parmon, V. N.; Elizarova, G. L.; Kim, T. V. *Ibid.* **1982**, *21*, 195. (e) Goswami, S.; Chakravarthy, A. R.; Chakravarthy, A. *J. Chem. Soc., Chem. Commun.* **1982**, 1288. (f) Shafrovich, V.Ya.; Strelets, V. V. *Nouv. J. Chim.* **1983**, *6*, 183. (g) Brunschwig, B. S.; Chou, M. H.; Cruetz, C.; Gosh, P. K.; Sutin, N. *J. Am. Chem. Soc.* **1983**, *105*, 4832. (h) Nord, G.; Pedersen, B.; Bjergbakke, E. *Ibid.* **1983**, *105*, 1913. (i) Nijs, H.; Fripiat, J. J.; Van Damme, H. *J. Phys. Chem.* **1983**, *87*, 1279. (j) Gosh, P. K.; Brunschwig, B. S.; Chan, M. H.; Creutz, C.; Sutin, N. *J. Am. Chem. Soc.* **1984**, *106*, 4772. (k) Baar, R. B.; Anson, F. C. *J. Electroanal. Chem.* **1985**, *187*, 265. (l) Taqui Khan, M. M.; Bhandwaj, R. C.; Jadhar, C. M. *J. Chem. Soc., Chem. Commun.* **1985**, 1650. (m) Ramaruj, R.; Kira, A.; Kaneko, M. *Angew. Chem., Int. Ed. Engl.* **1986**, *25*, 825.

(3) (a) Gersten, S. W.; Samuels, G. J.; Meyer, T. J. *J. Am. Chem. Soc.* **1982**, *104*, 4029. (b) Gilbert, J. A.; Eggleston, D. S.; Murphy, W. R.; Geselowitz, D. A.; Gersten, S. W.; Hodgson, D. J.; Meyer, T. J. *Ibid.* **1985**, *107*, 3855.

(4) Honda, K.; Frank, A. J. *J. Chem. Soc., Chem. Commun.* **1984**, 1635.

(5) Lay, P. S.; Sasse, W. H. F. *Inorg. Chem.* **1985**, *24*, 4707.

(6) Collins, J. P.; Sauvage, J. P. *Inorg. Chem.* **1986**, *25*, 135.

(7) Desilvestro, J.; Duonghong, D.; Kleijn, M.; Grätzel, M. *Chimia* **1985**, *4*, 102.

(8) Humphry-Baker, R.; Lilie, J.; Grätzel, M. *J. Am. Chem. Soc.* **1982**, *104*, 422, and references cited therein.

(9) Dwyer, F. P.; Goodwin, H. A.; Gyarfas, E. C. *Aust. J. Chem.* **1983**, *16*, 42, 544.

0002-7863/87/1509-6619$01.50/0

H_2SO_4 solutions containing peroxodisulfate. UV–visible absorption spectrophotometry, resonance Raman spectrophotometry, electrochemical measurements, HPLC, and elemental analysis indicated the formation of several oxo-bridged ruthenium dimers. In this report, we describe a new direct route for the preparation of this type of dimeric ruthenium complex involving the chemical synthesis of *cis*-$Ru^{II}L_2(H_2O)_2^{2+}$, followed by its electrochemical oxidative dimerization. We characterize intermediates and products by electrochemical and spectrophotometric techniques and examine the ability of the dimeric complex to function as an oxygen-evolution catalyst.

Experimental Section

Materials. (i) Synthesis of *cis*-$Ru^{II}L_2(H_2O)_2^{2+}$. The ligand 5,5′-dicarbethoxy-2,2′-bipyridine, L′, was prepared by dehydrogenative coupling of 30 g of ethyl nicotinate in the presence of 10 g of 10% Pd/charcoal (Fluka) under vacuum (15–20 mmHg) for 5 days at 125–130 °C. During filtration of the hot mixture, the crystalline solid separated. The crystals were washed with hexane and then extracted with toluene in a Soxhlet apparatus (27% yield; mp 145–147 °C). The NMR of the compound was consistent with the assigned structure (δ 4.45, $-CH_2$; 1.42, $-CH_3$, both parts of the ethyl group; 8.59 βH; 8.43 γH; 9.32 αH; solvent $CDCl_2$; internal standard Me_4Si). Also, the IR spectrum was identical with that of an authentic sample.

The ruthenium(II) complex $RuL'_2Cl_2 \cdot H_2O$ was prepared as follows: 390 mg (1.5 mmol) of $RuCl_3 \cdot 3H_2O$ (Fluka, 38–40% Ru) and 900 mg (3 mmol) of ligand L′ were dissolved in 100 mL of absolute EtOH; the mixture was refluxed under an Ar atmosphere for 24 h. After cooling, 50 mL of 1 M LiCl as added and the EtOH was evaporated under reduced pressure. The crystals were filtered off, washed with H_2O, and then air-dried (yield: >90%). The complex was recrystallized from hot EtOH. Elemental analysis gave good agreement with the expected values (weight percentages calculated for $C_{34}H_{32}N_4O_8Cl_2Ru \cdot H_2O$ are quoted in parentheses): C, 48.56 (48.61); H, 4.46 (4.33); N, 7.04 (7.09); Cl, 8.93 (8.97); Ru, 12.70 (12.79).

The complex *cis*-$Ru^{II}L_2Cl_2 \cdot 2.5H_2O$ was prepared by hydrolysis of $Ru^{II}L'_2Cl_2 \cdot H_2O$; 200 mg (0.25 mmol) of the latter was dissolved in a 1:1 (v/v) mixture of ethanol and water to which 260 mg of triethylamine (BDH >99%) was added. The mixture was refluxed for 24 h. Subsequently, 2 g (ca. 20 mmol) of HCl (Fluka puriss, 37%) was added and the solution reduced in the rotavap to a small volume. The product was left to crystallize in the dark for 24 h. The crystals were filtered off and dried in vacuo (yield >90%). In air, this compound adds lattice water. Elemental analysis for $C_{24}H_{16}N_4O_8Cl_2Ru \cdot 2.5H_2O$ gave: C, 41.05 (40.86); H, 3.09 (3.00); N, 7.97 (7.94); Cl, 10.16 (10.05); Ru, 14.91 (14.84).

Stock solutions of *cis*-$Ru^{II}L_2(H_2O)_2^{2+}$ were prepared from $Ru^{II}L_2Cl_2$ in 0.5 M H_2SO_4 (Fluka puriss grade) or 1 M trifluoromethanesulfonic acid (Fluka purum p.a. grade, further purified by vacuum distillation). The chloride ligands in the Ru^{II} complex were replaced by water ligands as follows. One mmole of silver sulfate (Fluka puriss.) was added to a H_2SO_4 solution of 1 mM $RuL_2Cl_2 \cdot 2.5H_2O$; when CF_3SO_3H was used as the solvent, 2 mmol of $AgCF_3SO_3$ (Fluka purum) was added. The solutions were heated for several hours to precipitate the chloride as AgCl. Subsequent filtration yielded the *cis*-$Ru^{II}L_2(H_2O)_2^{2+}$ solution that was used in the experiments. Care was taken to exclude light during this procedure and the stock solutions were stored in dark red bottles.

(ii) Synthesis of $Ru^{II}L_2SO_4 \cdot 4H_2O$. *cis*-$Ru^{II}L_2SO_4 \cdot 4H_2O$ precipitates slowly (weeks) from a 0.5–1.0 M H_2SO_4 solution of 2.5×10^{-3} M *cis*-$Ru^{II}L_2(H_2O)_2^{2+}$. The black crystals were filtered and washed with water, a water–ethanol mixture, and pure ethanol, and then air-dried. Elemental analysis for $C_{24}H_{16}N_4O_{12}Ru \cdot 4H_2O$ yielded: C, 38.03 (38.05); H, 3.26 (3.19); N, 7.44 (7.40). The IR spectrum of the sulfato complex exhibited S–O stretching frequencies at 1037, 1100, and 1260 cm^{-1}. The latter is characteristic[10] of bidentate chelation by SO_4^{2-} and suggests that both *cis*-$Ru^{II}L_2(H_2O)_2^{2+}$ and $Ru^{II}L_2SO_4$ have a cis configuration since SO_4^{2-} cannot coordinate to the trans isomer as a bidentate ligand. The assignment of the IR spectrum to the cis isomer concurs with spectrophotometric results discussed below.

(iii) Synthesis of $L_2(H_2O)Ru^{III}$–O–$Ru^{III}(OH_2)L_2Ba \cdot 13H_2O$. The dimer $L_2(H_2O)Ru^{III}$–O–$Ru^{III}(OH_2)L_2$ (1.25×10^{-3} M) was synthesized from a 0.5 M H_2SO_4 solution of 2.5×10^{-3} M *cis*-$Ru^{II}L_2(H_2O)_2^{2+}$ that was electrolyzed for 15 h at 40 °C as detailed in part iii of Results and Discussion. The dimer was isolated from solution as follows. A 625-mL portion of 0.02 M $Ba(OH)_2$ was injected slowly into 25 mL of the dimer solution until the pH reached ca. 3.5. $BaSO_4$ was removed by filtration and the volume of the solution was reduced to 10 mL in a rotavap (bath temperature ≤50 °C). A second 625-mL aliquot of 0.02 M $Ba(OH)_2$ was added to this solution, lowering the pH to about 3.5. The volume was concentrated to 10 mL and the $BaSO_4$ was removed by filtration. Next, acetone was added slowly to the stirred solution at room temperature, resulting in the precipitation of the dimer as the monobarium salt. The solution was left in the dark for about 24 h. Dark blue crystals of the dimer were collected by filtration and washed with a 4:1 mixture of acetone and water. Elemental analysis of the crystals for $C_{48}H_{30}N_8O_{19}Ru_2Ba \cdot 13H_2O$ yielded: C, 36.78 (36.11); N, 7.01 (7.02); H, 3.9 (3.6). The carbon-to-nitrogen ratio of 6.12 (calculated value, 6.0) indicates that no decarboxylation took place during the preparation of the dimer. Infrared analysis of the crystals revealed the presence of both COOH and COO^- groups and the absence of sulfate.

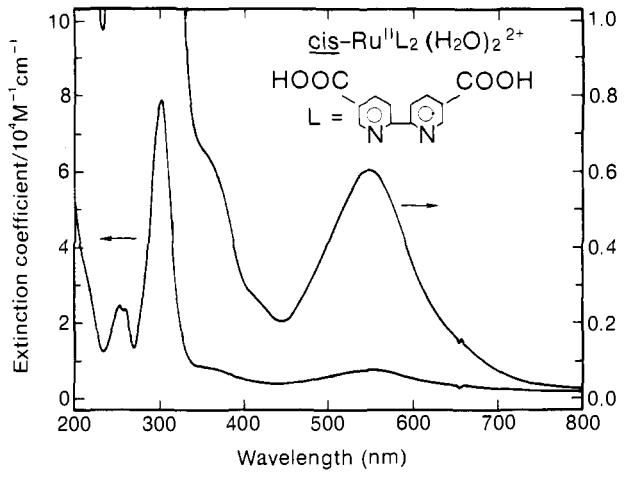

Figure 1. Absorption spectrum of 10^{-5} M [*cis*-$Ru^{II}L_2(H_2O)]^{2+}$ in 0.5 M H_2SO_4.

Apparatus. A Varian HPLC unit equipped with a Whatman "Partisil" anion-exchange column (30 × 0.4 cm, 5-μ particle size) was used to check the purity of solutions of the μ-oxo ruthenium ions. Initially, a variety of elution conditions were explored using phosphate and sulfate buffers and varying the pH and salt concentrations. Based upon the preliminary results obtained with the mixture of Ru–O–Ru dimers present in the photolyzed solutions of $RuL_3^{2+}/S_2O_8^{2-}/H_2SO_4$, an elution scheme was devised. Optimal separation of ruthenium-containing compounds of these product solutions was obtained by employing a linear 0.01–0.20 M HSO_4^-/SO_4^{2-} salt gradient at pH 2.4, applied over 6–20 min.

UV–visible absorption spectra were measured with a HP 8450A diode-array spectrophotometer. Raman spectra were obtained on an automated Jarrell-Ash Raman spectrophotometer using Spectra-Physics 164 Ar and Kr ion lasers and an RCA C31034 photomultiplier with photon-counting electronics.[11] Room-temperature Raman spectra were obtained from solutions contained within sealed capillary tubes (1.5–1.8-mm i.d.). The infrared spectra were measured on a Perkin-Elmer 684 spectrophotometer as KBr pellets. Electrochemical experiments employed a Wenking POS-73 potentiostat and a three-electrode, two-compartment cell. The working electrode for cyclic voltammetry was In-doped SnO_2 (0.7 cm^2 surface area; Balzers AG FL). Glassy carbon (0.3 cm^2 surface area) and basal plane graphite (0.2 cm^2 surface area) electrodes were employed in the rotating-disk studies. Controlled-potential electrolysis was performed with a Pt gauze electrode. A saturated $Na_2SO_4/HgSO_4/Hg$ reference electrode was employed to avoid chloride contamination. The solutions were deaerated by Ar bubbling. The electrode potentials reported in this paper are referenced to SCE.

Illuminations were performed with a 150-W tungsten–halogen lamp equipped with a water jacket and a 400-nm cutoff filter to remove infrared and ultraviolet radiation, respectively. The solution (10 mL) was contained in a 20-mL Pyrex glass vessel and was freed from oxygen by bubbling with Ar prior to photolysis. The solution temperature was maintained at 25 °C by means of a thermostat.

Oxygen production was monitored with a Clark-type membrane electrode (Yellow Springs Instruments, YSI Model 83) placed in the headspace above the solution. The results were corroborated by GC measurements; the GC was equipped with a thermal conductivity detector

(10) (a) Eskenazi, R.; Rasovan, J.; Levitus, R. *J. Inorg. Nucl. Chem.* **1986**, *28*, 521. (b) Ugo, R.; Conti, F.; Cenini, S.; Mason, R.; Robertson, G. B. *J. Chem. Soc., Chem. Commun.* **1968**, 1498. (c) Horn, R. W.; Weissberger, E.; Collman, J. P. *Inorg. Chem.* **1970**, *9*, 2367.

(11) Plowman, J. E.; Loehr, T. M.; Schauer, C. K.; Anderson, O. P. *Inorg. Chem.* **1984**, *23*, 3553.

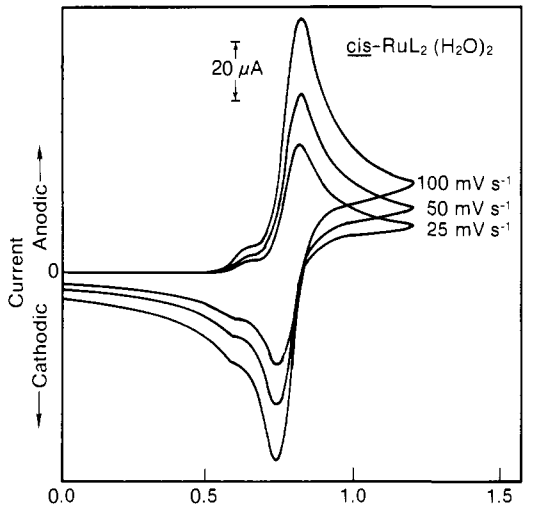

Figure 2. Cyclic voltammograms of 10^{-3} M $[cis\text{-}Ru^{II}L_2(H_2O)_2]^{2+}$ in 0.5 M H_2SO_4; In-doped SnO_2 working electrode (0.6 cm^2 area).

and Ar carrier gas. Air leakage was negligible on the time of the experiment and made no significant contribition to the observed oxygen-evolution rates.

Results and Discussion

(i) Spectral and Redox Properties of *cis*-$Ru^{II}L_2(H_2O)_2^{2+}$. Figure 1 shows the absorption spectrum of 10^{-5} M *cis*-$Ru^{II}L_2(H_2O)_2^{2+}$ in 0.5 M H_2SO_4. In the visible region, a broad band is observed with a maximum at 550 nm (ϵ 6000 M^{-1} cm^{-1}). This feature can be attributed to a $d_\pi(Ru) \rightarrow \pi^*$ (bipyridyldicarboxylic acid) transition. In the UV region, there is a shoulder at 365 nm and a very intense band at 300 nm (ϵ 8×10^4 M^{-1} cm^{-1}) which is ascribed to the ligand $\pi \rightarrow \pi^*$ transition. The complex exhibits almost identical absorption features in aqueous 1 M CF_3SO_3H; both the peak maxima and extinction coefficients were the same as those of the complex in 0.5 M H_2SO_4. The peak maxima of *cis*-$Ru^{II}L_2(H_2O)_2^{2+}$ are red shifted with respect to those of the unsubstituted analogue, *cis*-$Ru^{II}(bpy)_2(H_2O)_2^{2+}$, in 0.5 M CF_3COOH. In the case of *cis*-$Ru^{II}(bpy)_2(H_2O)_2^{2+}$, absorption bands are located at 480 nm (ϵ 8500 M^{-1} cm^{-1}), 335 (7700), and 290 (5×10^4).[12] This red shift is particularly striking for the $M \rightarrow L$ transition in the visible region, where the peak maximum is displaced by 70 nm. Apparently, the electron-withdrawing properties of the carboxylic acid groups lower the energy of the ligand acceptor orbitals.

Visible-light illumination of *cis*-$Ru^{II}L_2(H_2O)_2^{2+}$ solution leads to formation of a product with an absorption maximum at about 565 nm. We tentatively attribute these spectral changes to cis–trans isomerization. A similar reaction has been observed for $Ru^{II}(bpy)_2(H_2O)_2^{2+}$.[12] This process is relatively inefficient, since several hours of intense visible light illumination from a 450-W Xe lamp is required to convert $Ru^{II}L_2(H_2O)_2^{2+}$ from the cis to the trans isomer. *trans*-$RuL_2(H_2O)_2^{2+}$ and its dimeric forms are expected to display redox properties quite different from those of the cis isomers. This behavior was not further investigated in the present study. To avoid the cis–trans isomerization, the *cis*-$Ru^{II}L_2(H_2O)_2^{2+}$ solutions were protected from light.

Figure 2 shows cyclic voltammograms of *cis*-$Ru^{II}L_2(H_2O)_2^{2+}$ in deaerated 0.5 M H_2SO_4 solution. The current–voltage curves display oxidative and reductive peak potentials at 0.81 and 0.75 V, respectively. The 60-mV peak separation indicates a reversible one-electron oxidation of *cis*-$Ru^{II}L_2(H_2O)_2^{2+}$ to the corresponding Ru^{III} complex:

$$cis\text{-}Ru^{II}L_2(H_2O)_2^{2+} \rightleftharpoons cis\text{-}Ru^{III}L_2(H_2O)_2^{3+} + e^- \quad (1)$$

The halfwave redox potential E^0 derived from Figure 2 is 0.78 V (vs. SCE).

The effect of pH on the redox equilibrium could not be assessed because the *cis*-$Ru^{II}L_2(H_2O)_2^{2+}$ complex precipitated at pH >1. Presumably, deprotonation of the carboxylic acid substituents on the bipyridyl ligands produces the formally neutral zwitterionic form of the complex which is insoluble in water. The unsubstituted analogue, $[cis\text{-}Ru(bpy)_2(H_2O)_2]^{3+/2+}$, exhibits a formal potential of 0.53 V (vs. SCE) at pH 4 which increases with pH.[12] In the pH domain between 2 and 6, the potential changes by 59 mV for each unit change in pH. The pH dependence of the electrode potential was attributed to the deprotonation of the aqua ligands of the complex. At pH 2, the E^0 value for $[Ru(bpy)_2(H_2O)_2]^{3+/2+}$ in 0.5 M CF_3COOH is 0.63 V (vs. SCE), which is the same as that measured for the species in 1 M $HClO_4$ (0.63 V),[13] indicating that the complex is fully protonated at pH $\leq$2. By analogy, we assume that the two water ligands and carboxylic acid substituents of $[cis\text{-}RuL_2(H_2O)_2]^{3+/2+}$ in eq 1 do not undergo deprotonation in 0.5 M H_2SO_4. The formal charges cited on the formulas reflect these assumptions. For comparison, we also recorded the cyclic voltammogram of 10^{-3} M *cis*-$Ru^{II}(bpy)_2(H_2O)_2^{2+}$ in 0.5 M H_2SO_4. The halfwave potential for the $[cis\text{-}Ru(bpy)_2(H_2O)_2]^{3+/2+}$ couple was determined as 0.65 V, in agreement with previous measurements of the redox couple in 1 M $HClO_4$.[13] The 0.13-V positive shift of the E^0 of $[cis\text{-}RuL_2(H_2O)_2]^{3+/2+}$ (E^0 = 0.78 V) with respect to that of $[cis\text{-}Ru(bpy)_2(H_2O)_2]^{3+/2+}$ (E^0 = 0.65 V) is attributed to the electron-withdrawing properties of the COOH substituents. This effect is even more pronounced for the ruthenium trisbipyridyl complexes, where the introduction of the carboxylic acid groups at the 5,5′ positions of the bipyridyl ligands increases the redox potential by 300 mV, i.e., from 1.02 to 1.32 V, with respect to the unsubstituted analogue, $Ru(bpy)_3^{2+}$.

In addition to the prominent peaks associated with the electrochemistry of $[cis\text{-}RuL_2(H_2O)_2]^{3+/2+}$, a second much smaller reversible wave at 0.63 V appears in the cyclic voltammograms in Figure 2. With aqueous CF_3SO_3H as the solvent, the latter feature was absent, and only the reversible wave at 0.78 V due to the oxidation of *cis*-$Ru^{II}L_2(H_2O)_2^{2+}$ was observed. The background current for sulfuric acid alone stayed below 1 μA over the entire potential range. Thus, it is unlikely that the reversible wave at 0.63 V arises from an impurity. One possibility is that the wave is produced by adsorbed complexes at the In-doped SnO_2 surface. However, when the current–voltage measurements were repeated with different electrode materials (basal plane graphite, glassy carbon, and Pt) in H_2SO_4 and in CF_3SO_3H solutions containing *cis*-$Ru^{II}L_2(H_2O)_2^{2+}$, the cyclic voltammograms obtained were the same as those with In-doped SnO_2. Since the reversible wave at 0.63 V was absent in CF_3SO_3H but was present in H_2SO_4, we investigated the possibility that the electroactive species might be a sulfato complex, arising from the ligand exchange of SO_4^{2-} for water.

$$cis\text{-}RuL_2(H_2O)_2^{2+} + SO_4^{2-} \rightleftharpoons cis\text{-}RuL_2SO_4 + 2H_2O \quad (2)$$

An authentic sample of *cis*-$Ru^{II}L_2SO_4$ gave a current–voltage response that was consistent with the assignment of the reversible wave at 0.63 V to the sulfato complex. Sulfate ligation has been proposed for similar polypyridyl ruthenium complexes.[14,15]

The electrochemical oxidation of *cis*-$Ru^{II}L_2(H_2O)_2^{2+}$ was further investigated by a rotating disk (basal plane graphite, 0.20 cm^2 surface area) electrode. In these studies, 0.5 M H_2SO_4 solutions contained 10^{-3} M *cis*-$Ru^{II}L_2(H_2O)_2^{2+}$, and the rotational speed of the electrode was varied between 200 and 2000 rpm. The current associated with the oxidation of *cis*-$Ru^{II}L_2(H_2O)_2^{2+}$ was found to vary as the square root of the rotational speed, indicating a diffusion-controlled process. Moreover, from the slope of a Koutecky–Levich plot, it was determined that one electron was transferred during oxidation of the complex (see eq 1) and that the diffusion coefficient of *cis*-$Ru^{II}L_2(H_2O)_2^{2+}$ was 2.4×10^{-6} cm^2 s^{-1}. For comparison, rotating-disk studies of the one-electron

(12) Durham, B.; Wilson, S. R.; Hodgson, D. J.; Meyer, T. J. *J. Am. Chem. Soc.* **1980**, *102*, 600.

(13) Takeuchi, K. J.; Samuels, G. J.; Gersten, S. W.; Gilbert, J. A.; Meyer, T. J. *Inorg. Chem.* **1983**, *22*, 1049.

(14) McHatton, R. C.; Anson, F. C. *Inorg. Chem.* **1984**, *23*, 3935.

(15) Haas, O.; Zumbrunnen, H. R.; Vos, J. G. *Electrochim. Acta* **1985**, *30*, 1551.

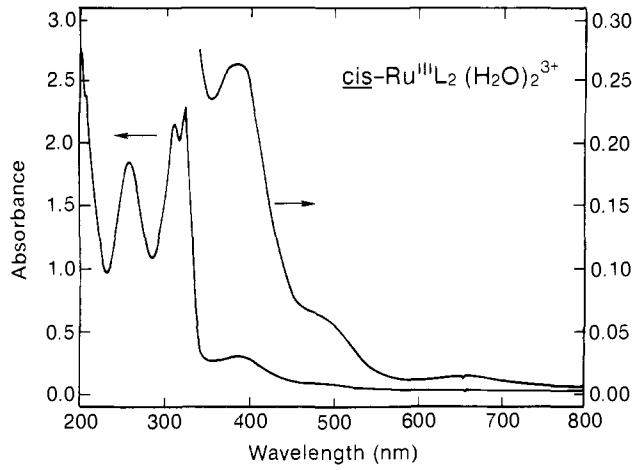

Figure 3. Absorption spectrum of 3.2×10^{-4} M *cis*-$Ru^{III}L_2(H_2O)_2^{3+}$ in 0.5 M H_2SO_4; 0.1-cm optical path length.

oxidation of $Ru(bpy)_3^{2+}$ performed with the same electrode yielded a diffusion coefficient of 3×10^{-6} cm^2 s^{-1}.

In Figure 2 the electrode potential was scanned between 0 and 1.2 V. When the In-doped SnO_2 electrode was polarized to more positive potentials, the anodic current increased sharply above 1.4 V, passing through a maximum at about 1.5 V and declining thereafter. On the reverse scan, a cathodic peak was observed at about 0.8 V in addition to the reduction wave of $Ru^{III}L_2(H_2O)_2^{3+}$ shown in Figure 2. This behavior can be ascribed to the formation of complexes for which the oxidation state of Ru exceeds III.[16] The cyclic voltammogram shows a crossover feature, suggesting that the oxidation of *cis*-$RuL_2(H_2O)_2$ in the 1.4–1.6-V region leads to the formation of products that undergo nucleation and phase growth at the In-doped SnO_2 electrode surface.[17]

(ii) **Spectral Properties of *cis*-$Ru^{III}L_2(H_2O)_2^{3+}$.** Quantitative oxidation of *cis*-$Ru^{II}L_2(H_2O)_2^{2+}$ to *cis*-$Ru^{III}L_2(H_2O)_2^{3+}$ was carried out by controlled-potential electrolysis at 1.1 V using a Pt gauze electrode as follows. A 15-mL 0.5 M H_2SO_4 solution of 4.8×10^{-4} M $Ru^{II}L_2(H_2O)_2^{2+}$ was placed in a double-walled Pyrex cell connected to a thermostat adjusted to 25 °C. The solution was protected from light to avoid cis–trans isomerization during the electrolysis. The cell was purged continuously with Ar to prevent reduction of the Ru^{III} complex by hydrogen formed at the counter electrode. After 1.5 h of electrolysis, the current had declined to less than 10% of its initial value and the color of the solution had changed from deep purple to faint yellow. The absorption spectrum of the product solution (Figure 3) displays peak maxima at 262 nm (ϵ 3.6×10^4 M^{-1} cm^{-1}), 314 (4.3×10^4), 326 (4.6×10^4), and 390 (5.5×10^3). These spectral features are similar to those of *cis*-$Ru^{III}(bpy)_2(H_2O)_2^{3+}$ in 0.5 M CF_3COOH which have maxima at 247, 300, and 312 nm.[12] As with the Ru^{II} analogues, the effect of COOH substitution at the 5,5′ positions of the bipyridyl ligands is to shift the absorption bands to longer wavelengths. In Figure 3 one can also notice very weak absorptions around 650 and 500 nm. As discussed below, these arise from dimeric Ru complexes formed in very small concentration during the electrochemical oxidation.

(iii) **Synthesis and Electrochemical Characterization of $L_2(H_2O)Ru$–O–$Ru(H_2O)L_2$.** Quantitative dimerization of *cis*-$Ru^{II}L_2(H_2O)_2^{2+}$ was obtained by oxidative electrolysis of the solution characterized in Figure 3 with the following alteration in conditions. The concentration of the *cis*-$Ru^{II}L_2(H_2O)_2^{2+}$ solution was changed from 4.8×10^{-4} to 2.5×10^{-3} M, the temperature was raised from 25 to 40 °C, and the electrolysis time was extended from 1.5 to 15 h. At the end of the electrolysis, the color of the solution had changed from purple to red. The

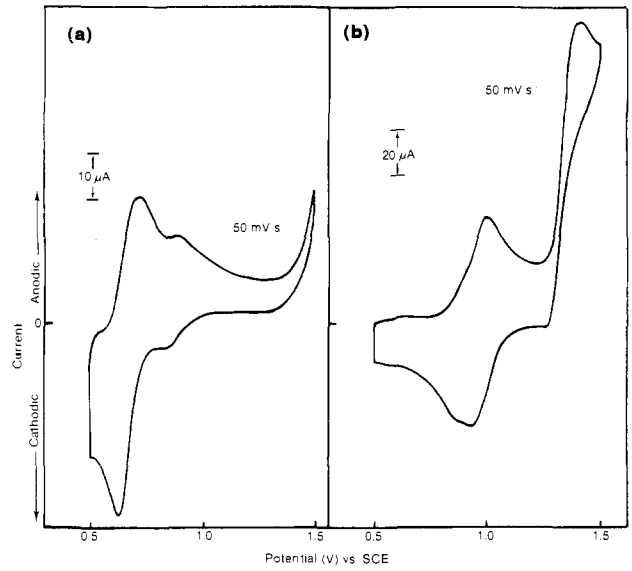

Figure 4. Cyclic voltammograms of product solutions from electrolysis of *cis*-$Ru^{II}L_2(H_2O)_2^{2+}$ in 0.5 M H_2SO_4; In-doped SnO_2 working electrode (0.6 cm^2 area). The background current was below 1 μA throughout the potential range: (a) after electrolysis, solution contains sulfato complexes of Ru^{III}–O–Ru^{IV}; (b) after solution a was poised at 0.65 V until nearly complete conversion of sulfato complexes of Ru^{III}–O–Ru^{IV} to diaqua form of Ru^{III}–O–Ru^{III}.

cyclic voltammogram shown in Figure 4a exhibits a quasi-reversible wave centered at 680 mV (100-mV peak separation), a smaller reversible wave centered at 870 mV (60-mV peak separation), and the onset of a catalytic wave at potentials more positive than 1.35 V at a scan rate of 50 mV s^{-1}. As discussed below, these features are attributed to sulfato complexes of the mixed-valence dimer Ru^{III}–O–Ru^{IV}. (For convenience, the oxidation states of the dimer are denoted by formulas such as Ru^{III}–O–Ru^{IV}.)

Upon reduction of the Ru^{III}–O–Ru^{IV} dimer by electrolysis at 0.65 V, the color of the solution changed from red to deep blue-green. The cyclic voltammogram of this solution (Figure 4b) is strikingly different from that obtained prior to reduction. The two principal features are a reversible wave at 0.98 V and a pronounced catalytic wave for oxygen production starting at 100–200 mV positive of the standard water–oxidation potential. There is also a shoulder on the cathodic part of the main wave at 870 mV. The corresponding anodic hump is barely visible. Furthermore, a very small wave centered at 0.6 V is discernible. The difference in the cyclic voltammograms obtained prior and subsequent to reduction are attributed to the replacement of sulfate by water ligands upon conversion of Ru^{III}–O–Ru^{IV} to Ru^{III}–O–Ru^{III}.

In order to confirm this assignment, the dimerization was performed with aqueous CF_3SO_3H as the solvent: 10^{-3} M $Ru^{II}L_2(H_2O)_2^{2+}$ in 0.5 M CF_3SO_3H was electrolyzed at 1.1 V and 25 °C for 24 h and then at 41 °C for another 24 h to complete the oxidative dimerization. At the end of electrolysis, the solution exhibited the characteristic red color of the Ru^{III}–O–Ru^{IV} dimer which changed spontaneously within hours to the blue-green color of Ru^{III}–O–Ru^{III}. The current–voltage curves of the oxidized and reduced forms of the dimer were identical (Figure 5). The cyclic voltammogram exhibits, apart from the catalytic wave, a reversible wave at $E^0 = 0.98$ V, corresponding to the redox equilibrium between Ru^{III}–O–Ru^{III} and Ru^{IV}–O–Ru^{III} dimers:

$$Ru^{III}\text{–O–}Ru^{III} \underset{e^-}{\overset{-e^-}{\rightleftharpoons}} Ru^{III}\text{–O–}Ru^{IV} \qquad (3)$$

Other waves that are observed in Figure 4 at lower potentials probably arise from dimers, where one or both water ligands have been replaced by sulfate or bisulfate. Complexes with different structures are possible since sulfate can coordinate to Ru as either a monodentate or a bidentate ligand. Ru^{III}–O–Ru^{III} seems to coordinate sulfate much less strongly than Ru^{III}–O–Ru^{IV}, as is

(16) For recent information on high-valent oxo-ruthenium complexes of 2,2′-bipyridine, cf.: Che, C. H.; Wang, K. Y.; Leung, W. H.; Poon, C. K. *Inorg. Chem.* **1986**, *25*, 345, and references cited therein.

(17) Fleischmann, M.; Comte, P.; Grätzel, M., unpublished results.

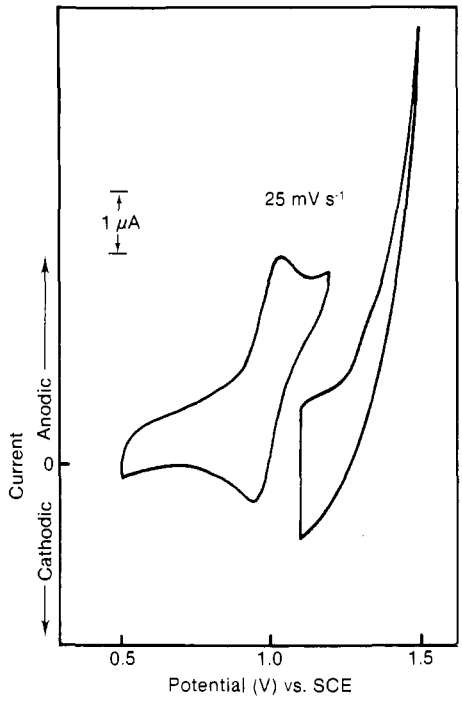

Figure 5. Cyclic voltammogram of 5×10^{-4} M Ru^{III}–O–Ru^{IV} in aqueous 0.5 M CF_3SO_3H; In-doped SnO_2 working electrode (0.6 cm^2 area). The background current was below 1 μA throughout the potential range.

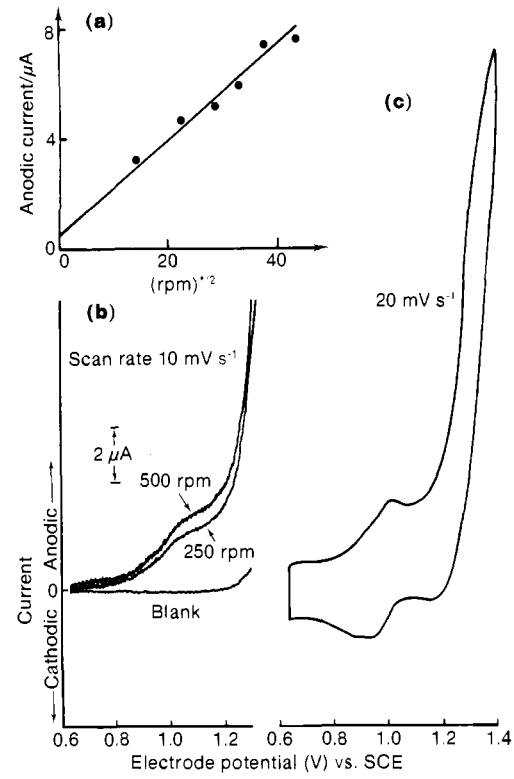

Figure 6. Rotating-disk electrode studies of 2.2×10^{-4} M $L_2(H_2O)Ru$–O–$Ru(H_2O)L_2$ in 0.5 M H_2SO_4; basal plane graphite disk electrode (0.2 cm^2 area): (a) current–potential diagram obtained at rotating speeds of 250 and 500 rpm; (b) Levich plot of the plateau current of the first wave (E^0 = 0.98 V (vs. SCE)) as a function of rotational speed; (c) cyclic voltammogram with the electrode at rest.

evident from the prominence of the 0.98-V wave in the cyclic voltammogram in Figure 4b. Presumably, the high electrophilicity of the Ru centers in the mixed-valence state favors sulfate coordination. The replacement of water ligands by sulfate in the mixed-valence dimer is a relatively slow process as shown by the following experiment.

Bulk electrolysis (at 1.1 V) of Ru^{III}–O–Ru^{III} in 0.5 M H_2SO_4 quantitatively converts it back to the mixed-valence Ru^{III}–O–Ru^{IV} state. The Faradaic charge passed during oxidation correlates with a one-electron process. If the oxidation is carried out sufficiently fast, i.e., within ca. 1 h, the cyclic voltammogram of the Ru^{III}–O–Ru^{IV} dimer is the same as that displayed in Figure 4b. Owing to the replacement of water by sulfate ligands, there is a slow change in the current–voltage curve upon maintaining the solution at a potential of 1.1 V. After 2 days, the features reverted to those shown in Figure 4a, indicating that sulfate coordination to Ru^{III}–O–Ru^{IV} was complete. When this solution was again reduced at 0.65 V, the cyclic voltammogram shown in Figure 4b was reproduced.

Similar to the behavior observed in aqueous CF_3SO_3H, the Ru^{III}–O–Ru^{IV} dimer produced by rapid electrochemical or chemical oxidation of Ru^{III}–O–Ru^{III} in aqueous 0.5 M H_2SO_4 undergoes spontaneous reduction back to the Ru^{III}–O–Ru^{III} state within a few hours. When the dimer was maintained in the mixed-valence state for a longer period, e.g., by poising the solution potential at 1.1 V for several days, the spontaneous transformation of the III–IV state to the III–III state was no longer observed; the III–IV state appears stable for at least several months. Such stability can be rationalized in terms of the difference in the redox potentials between the diaqua and the sulfato complexes of the mixed-valence dimer. Freshly prepared, the mixed-valence dimer exhibits a standard redox potential of 0.98 V (Figure 4b). Upon aging for several days in 0.5 M H_2SO_4, sulfato complexes of the dimer are formed and the respective current maxima shift to 0.68 and 0.87 V, corresponding to those in Figure 4a. The lowering of the redox potential accounts for the increased stability of the aged dimer.

Characterization of the electrochemical properties of the dimeric complex in 0.5 M H_2SO_4 was pursued using a rotating basal plane graphite disk electrode. Figure 6b shows current–potential curves obtained at rotational speeds of 250 and 500 rpm, respectively. Two waves are clearly distinguishable. The first one has a halfwave potential of 0.98 V (vs. SCE) and the plateau current increases with the square root of the rotational speed in agreement with the Levich equation, Figure 6a. Using a diffusion coefficient of 1.2×10^{-6} cm^{-2} s^{-1} for the dimer, which corresponds to half of the value determined for the *cis*-$Ru^{II}L_2(H_2O)_2^{2+}$ monomer, one electron is calculated to be transferred in the electrochemical reaction. This finding confirms that the reversible wave at 0.98 V is due to the one-electron oxidation of Ru^{III}–O–Ru^{III} to produce the mixed-valence Ru^{III}–O–Ru^{IV} dimer. Figure 6b shows a steep increase in the anodic current at potentials positive to 1.1 V. In this potential domain, the current shows little dependence on the rotational speed, indicating that the wave corresponds to a catalytic process. The catalytic wave is also observed by cyclic voltammetry performed with the quiescent graphite electrode (Figure 6c). The features of this voltammogram are the same as those observed with an In-doped SnO_2 electrode (Figure 4b). In particular, the reversible wave occurs at 0.98 V, corresponding to the one-electron oxidation of Ru^{III}–O–Ru^{III} to produce the mixed-valence Ru^{III}–O–Ru^{IV} dimer.

Solid Ru^{III}–O–Ru^{III} was isolated from 0.5 M H_2SO_4 solution as described in the Experimental Section. The dimer was precipitated as the monobarium salt, i.e., $L_2(H_2O)Ru^{III}$–O–$Ru^{III}(H_2O)L_2Ba \cdot 13H_2O$ at pH ~3.5 after removal of H_2SO_4 with diluted $Ba(OH)_2$. The absence of sulfate in the solid material was confirmed by IR spectroscopy.

(iv) Spectral Characterization of the Ru^{III}–O–Ru^{III} and Ru^{III}–O–Ru^{IV} Dimers in Acidic Solution. 1. UV–Visible Absorption Spectra. The absorption spectrum of Ru^{III}–O–Ru^{III} in 0.5 M H_2SO_4 is shown in Figure 7a. It exhibits a strong symmetric absorption peak at 654 nm (ϵ 1.8×10^4 M^{-1} cm^{-1}) in the visible region and two peaks at 257 nm (ϵ 5.5×10^4 M^{-1} cm^{-1}) and 296 nm (ϵ 7×10^4 M^{-1} cm^{-1}) in the ultraviolet region. The absorption spectrum is similar to that of the unsubstituted analogue,[3b] $[(bpy)_2(H_2O)Ru^{III}$–O–$Ru^{III}(H_2O)(bpy)_2]^{4+}$, except that all the maxima are red shifted with respect to the unsubstituted complex.

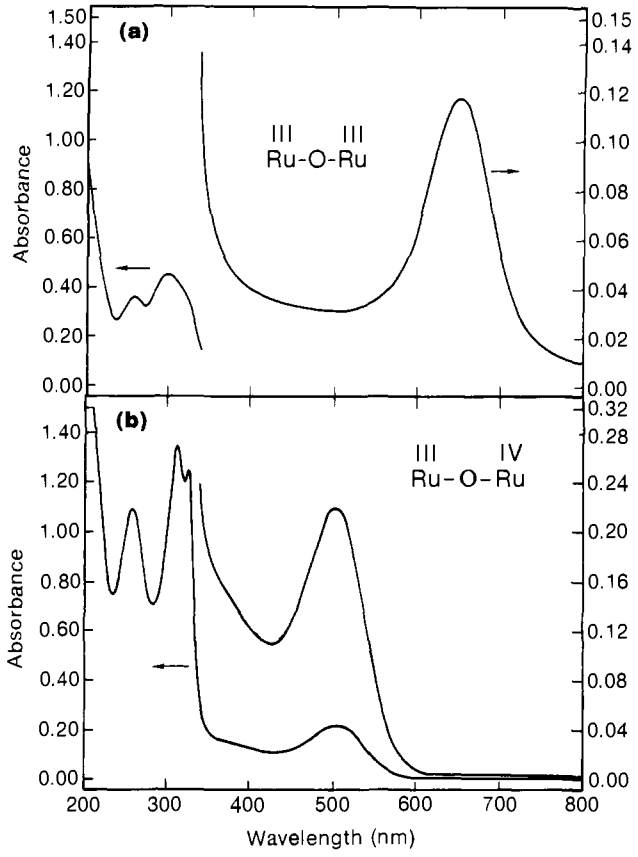

Figure 7. (a) Absorption spectrum of 3.3×10^{-5} M oxo-bridged dimer $L_2(H_2O)Ru^{III}$–O–$Ru^{III}(H_2O)L_2$ in 0.5 M H_2SO_4; 0.2-cm optical path-length. (b) Absorption spectrum of 1.3×10^{-5} M Ru^{III}–O–Ru^{IV} in 0.5 M H_2SO_4; 1.0-cm optical path length.

The Ru^{III}–O–Ru^{III} dimer is cleaved by reductants such as ascorbic acid. When 90 μL of 10^{-2} M ascorbic acid in water was added to 100 μL of 1.25×10^{-3} M $L_2(H_2O)Ru^{III}$–O–$Ru^{III}(H_2O)L_2$ in 0.5 M sulfuric acid, the solution turned purple within a few minutes and its spectrum was identical with that depicted in Figure 1 for *cis*-$Ru^{II}L_2(H_2O)_2^{2+}$. Spectrophotometric analysis showed that the reductive cleavage of the dimer was quantitative:

$$L_2(H_2O)Ru^{III}\text{–}O\text{–}Ru^{III}(H_2O)L_2 \xrightarrow[H_2O]{2e^-,\, nH^+} 2cis\text{-}Ru^{II}L_2(H_2O)_2^{2+} \quad (4)$$

The charge of Ru^{III}–O–Ru^{III} is unspecified because the degree of protonation of the carboxyl groups of the dimer in aqueous 0.5 M H_2SO_4 is uncertain. The water ligands of Ru^{III}–O–Ru^{IV} may also undergo deprotonation in 1 N acid. In the case of the unsubstituted analogues[3b] $[(bpy)_2(H_2O)Ru^{III}\text{–}O\text{–}Ru^{III}(H_2O)(bpy)_2]^{4+}$ and $[(bpy)_2(H_2O)Ru^{III}\text{–}O\text{–}Ru^{IV}(H_2O)(bpy)_2]^{5+}$, the water ligands undergo deprotonation above pH 6 and 0.4, respectively.

The UV–visible absorption spectrum of the mixed-valence dimer was obtained from a solution prepared by chemical oxidation of Ru^{III}–O–Ru^{III} with Co^{3+} ions in 0.5 M H_2SO_4. The cobaltic solution is particularly appropriate for spectral analysis since the absorption spectrum of both Co^{3+} and Co^{2+}, at the concentrations employed, contribute negligibly to that of the dimer in the visible and UV regions of interest. A stock solution of cobaltic ions was prepared in 3 M H_2SO_4 by bulk electrolysis of 4×10^{-2} M $CoSO_4$. Typically, 50% of the Co^{2+} ions were oxidized to Co^{3+} and the solution was stored under refrigeration. A 2-mL sample containing ca. 2×10^{-5} M Ru^{III}–O–Ru^{III} was mixed with the Co^{3+}, which was added in slight excess of the stoichiometric amount. Upon addition of Co^{3+}, the color of the solution changed immediately from blue-green to red. The absorption spectrum of the product in Figure 7b shows a symmetric peak at 500 nm in the visible region and peaks at 258, 313, and 325 nm in the UV region and

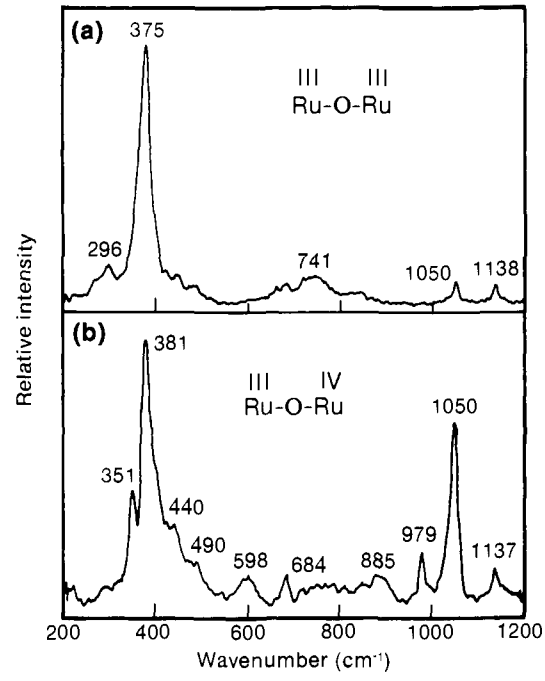

Figure 8. (a) Resonance Raman spectrum of $L_2(H_2O)Ru^{III}$–O–$Ru^{III}(H_2O)L_2$ in 0.5 M H_2SO_4 with excitation at 647.1 nm, using the Kr ion laser at 40 mW power, 5-cm^{-1} slit width, scan rate of 1 cm^{-1} s^{-1}; average of two scans, 13-points smoothing routine applied, spectrum background subtracted, 90° scattering geometry. (b) Resonance Raman spectrum of Ru^{III}–O–Ru^{IV} with excitation at 514.5 nm, using the Ar ion laser at 30-mW power, single scan, 21 point smoothing routine applied. Other conditions are as in (a).

is identified as that of the mixed-valence dimer Ru^{III}–O–Ru^{IV}. Similar to the situation of Ru^{III}–O–Ru^{III}, all the absorption maxima of Ru^{III}–O–Ru^{IV} red shifted with respect to the unsubstituted analogue,[3b] $[(bpy)_2(H_2O)Ru^{III}\text{–}O\text{–}Ru^{IV}(H_2O)(bpy)_2]^{5+}$. The extinction coefficients of Ru^{III}–O–Ru^{IV} were determined as ϵ 8.5×10^4 M^{-1} cm^{-1} (258 nm), 1×10^5 (313), 9.5×10^4 (325), and 1.7×10^4 (500). The replacement of water ligands by sulfate and/or bisulfate does not lead to large changes in the UV–visible spectrum of the mixed-valence dimer.

2. Resonance Raman Spectroscopy. Spectra of Ru^{III}–O–Ru^{III} and Ru^{III}–O–Ru^{IV} in aqueous 0.5 M H_2SO_4 were recorded under both resonance and off-resonance conditions. The resonance spectrum of Ru^{III}–O–Ru^{III}, obtained from 647.1-nm excitation (Figure 8a), exhibits a single sharp peak at 375 cm^{-1} and much smaller bands at 296, 741, 1050, and 1148 cm^{-1}. The off-resonance spectrum of Ru^{III}–O–Ru^{III}, obtained with 520.8-nm excitation, shows only a very weak feature in the 350- to 500-cm^{-1} region, indicating that the 375-cm^{-1} line is resonance enhanced. Also, the 375-cm^{-1} line showed a polarization ratio of 0.33 which is the expected value for a resonance enhanced signal.

On the basis of an extensive data base for oxo-bridged metal complexes,[11,18-20] one can infer that the 350- to 500-cm^{-1} wavenumber region corresponds to the Raman active M–O–M symmetric stretching frequency ν_s. For example, ν_s (Fe–O–Fe) of (μ-oxo)bis(aquobis(phenanthroline)iron(III)) occurs at 363 cm^{-1}.[11] The feature at 375 cm^{-1} is therefore assigned to the Raman-active (Ru–O–Ru) symmetric stretching frequency mode. One-electron oxidation of Ru^{III}–O–Ru^{III} by Ce^{4+} to the mixed-valence dimer shifts this resonance line to 381 cm^{-1} as illustrated in Figure 8b. In the case of Ru^{III}–O–Ru^{IV}, resonance excitation was at 514.5 nm. Other peaks in this spectrum are assigned to HSO_4^- (1050, 885, 598 cm^{-1}), SO_4^{2-} (979 cm^{-1}), and bipyridyl ligand modes

(18) Burke, J. J.; Kincaid, J. R.; Spiro, T. G. *J. Am. Chem. Soc.* **1978**, *100*, 6077.
(19) San Filippo, J., Jr.; Grayson, R. L.; Sniadock, H. T. *Inorg. Chem.* **1976**, *15*, 1103.
(20) Campbell, J. R.; Clark, R. J. H. *J. Chem. Soc., Faraday Trans. 2* **1980**, *76*, 1103.

Scheme I

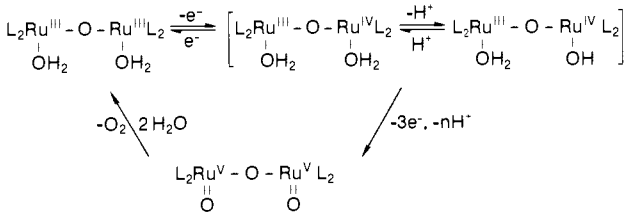

Scheme II

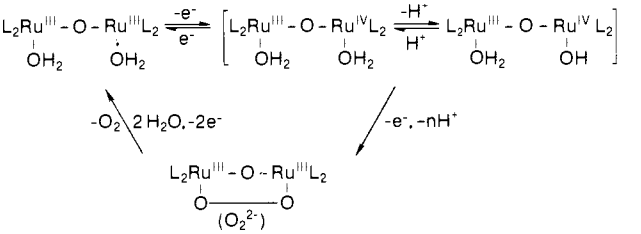

(1137 cm^{-1}). The shoulder at 351 cm^{-1} may be due to a fraction of Ru^{III}–O–Ru^{IV} species which exists as a sulfato complex. These results confirm that the 650- and 500-nm absorption bands in Figure 7 are due to μ-oxo complexes.

Resonance Raman studies were also carried out on 0.5 M H_2SO_4 solutions of RuL_3^{2+} with peroxodisulfate that had been illuminated by visible light or subject to thermolysis at 80 °C. These studies provided unambiguous evidence for the formation of oxo-bridged ruthenium complexes. We assume that the dimers are formed via reactions 5 to 7:

$$2RuL_3^{2+} + S_2O_8^{2-} \xrightarrow[\text{heat}]{\text{light or}} 2RuL_3^{3+} + 2SO_4^{2-} \quad (5)$$

$$RuL_3^{3+} + 2H_2O \rightarrow RuL_2(H_2O)_2^{3+} + L \quad (6)$$

$$2RuL_2(H_2O)_2^{3+} \rightarrow L_2(H_2O)Ru^{III}\text{–}O\text{–}Ru^{III}(OH_2)L_2 + H_2O + nH^+ \quad (7)$$

Further oxidation of Ru^{III}–O–Ru^{III} by peroxodisulfate to form Ru^{III}–O–Ru^{IV} is also observed. The resonance Raman spectrum of product solutions showed at least four lines in the 350- to 500-cm^{-1} wavenumber region, suggesting the formation of several Ru–O–Ru dimers with differing ligand composition and/or geometrical isomerism.

3. HPLC Analysis. A 100-μL aliquot of 3×10^{-4} M Ru^{III}–O–Ru^{III}, obtained by electrolysis of *cis*-$Ru^{II}L_2(H_2O)_2^{2+}$, was injected onto the Whatman "Partisil" ion-exchange column and eluted with HSO_4^-/SO_4^{2-} salt gradient at pH 2.4. The elution products were detected at 670 and 320 nm. At both wavelengths only one major peak with a shoulder was observed, having retention times of 11.34 and 13.17 min, respectively. An aliquot of the photolyzed solution of $RuL_3^{2+}/S_2O_8^{2-}$ was also analyzed. In this case, the chromatogram exhibited at least eight different peaks, revealing the presence of several oxo-bridged ruthenium complexes.

(v) Catalysis of Oxygen Generation from Water. The catalytic activity of Ru–O–Ru toward oxidation of water to oxygen was examined in electrochemical, thermochemical, and photochemical experiments.

1. Electrochemical Water-Oxidation Studies. The cyclic voltammograms in Figures 4–6 show large catalytic waves with an onset that is 100–200 mV positive of the reversible electrode potential for oxygen evolution. The appearance of the high anodic current close to the thermodynamic threshold signifies efficient water-oxidation catalysis by the carboxylated ruthenium dimer. The kinetics for the catalytic oxidation of water with the carboxylated dimer are considerably more favorable than those with $[(bpy)_2(H_2O)Ru\text{–}O\text{–}Ru(OH_2)(bpy)_2]^{4+}$. The latter system exhibits sluggish kinetics for O_2 production even at optimum pH conditions.[4] At scan rates of 50 mV s^{-1}, $[(bpy)_2(H_2O)Ru\text{–}O\text{–}Ru(OH_2)(bpy)_2]^{4+}$ shows no catalytic wave for the oxidation of water on a glassy carbon electrode.[3] In marked contrast, $L_2(H_2O)Ru\text{–}O\text{–}Ru(OH_2)L_2$ exhibits a catalytic wave for O_2 evolution from water at scan rates up to 2000 mV s^{-1} (maximum sweep rate used) that suggests that the catalysis for O_2 production can occur in the millisecond-to-submillisecond time regime.

At present, the detailed mechanism for the water-oxidation reaction has not been investigated. We suggest, nevertheless, two plausible models for the operation of the catalyst (Schemes I and II). Scheme I is the same as the mechanism proposed for the unsubstituted dimer.[3b] It involves the one-electron oxidation of the Ru^{III}–O–Ru^{III} dimer to the Ru^{III}–O–Ru^{IV} complex at $E_{1/2}$ = 0.98 V. In the potential range of the catalytic wave, successive removal of electrons and protons yields a higher oxidized intermediate, presumably a Ru^{V}–O–Ru^{V} dimer that reverts to the Ru^{III}–O–Ru^{III} valence state upon elimination of molecular oxygen.

Scheme II differs from Scheme I in that a μ-peroxo complex is formed presumably from the Ru^{IV}–O–Ru^{IV} dimer. Upon further oxidation, this complex releases oxygen with simultaneous reformation of the Ru^{III}–O–Ru^{III} dimer.

2. Chemical Water Oxidation. Dropwise addition of a mixture of 2×10^{-2} M Co^{3+} and 2×10^{-2} M Co^{2+} ions in 3 M H_2SO_4 to 2.5×10^{-5} M $L_2(H_2O)Ru^{III}\text{–}O\text{–}Ru^{III}(H_2O)L_2$ in deaerated 1 M H_2SO_4 resulted in the immediate appearance of the characteristic red color of the mixed-valence dimer. The spectrum of Ru^{III}–O–Ru^{IV} persisted even after the addition of a 300-fold stoichiometric excess of Co^{3+}. The excess Co^{3+} ions were reduced rapidly to Co^{2+} ions with simultaneous evolution of oxygen. The generation of oxygen was monitored quantitatively with a Clark-type O_2 sensor located in the head space of the cell. The production of O_2 was further corroborated by gas chromatography. The reaction was terminated after ca. 1 h. During this period, about 500 μL of O_2 had evolved. The amount of O_2 evolved and Co^{3+} reduced corresponded to the stoichiometry of the reaction:

$$4Co^{3+} + 2H_2O \rightarrow O_2 + 4Co^{2+} + 4H^+ \quad (8)$$

In the absence of Ru^{III}–O–Ru^{III}, the reduction of Co^{3+} by water is a slow process requiring many hours under our experimental conditions (1 M H_2SO_4 and 25 °C). Thus, a concentration of 2.5×10^{-5} M Ru–O–Ru dimer is sufficient to accelerate markedly the water-oxidation reaction. The most striking aspect of this oxygen-evolution catalyst is its stability under the strongly oxidizing conditions prevailing in the acidic $Co^{3+/2+}$ solution, the electrochemical potential of which is about 1.5 V (vs. SCE). After complete conversion of Co^{3+} to Co^{2+} in the water-oxidation reaction, the turnover number of the Ru–O–Ru dimer was 75 with respect to O_2 production, and there were no signs of degradation. Specifically, the spectral features were unchanged and the absorbance of Ru^{III}–O–Ru^{IV} at 500 nm remained within 10% of its original value; the spectrum was corrected for the contribution of Co^{2+}. This contrasts to the behavior of the unsubstituted dimer $[(bpy)_2(H_2O)Ru^{III}\text{–}O\text{–}Ru^{IV}(OH_2)(bpy)_2]^{5+}$ which was investigated under the same conditions. In the case of $[(bpy)_2(H_2O)Ru^{III}\text{–}O\text{–}Ru^{IV}(OH_2)(bpy)_2]^{5+}$, substantial irreversible spectral changes occurred during O_2 evolution, indicating degradation of this complex.

Oxygen evolution was also observed in 0.5 M H_2SO_4 solution containing Ce^{4+} and small amounts of Ru^{III}–O–Ru^{III}. Upon addition of 2×10^{-7} mol of Ru^{III}–O–Ru^{III} to 10 mL of 0.1 M $Ce(SO_4)_2$ in 0.5 M H_2SO_4, oxygen was generated at an initial rate of 40 μL h^{-1}. The rate declined to ca. 10% of this value after a few hours. This decrease was likely due to the slow replacement of water ligands in the mixed-valence dimer by sulfate and possibly due to complexation of the carboxyl groups of the bipyridyl ligands with Ce^{3+}. These sulfato complexes exhibit a much lower activity as oxygen-evolution catalysts than the dimer with aqua ligands and were essentially inactive in promoting water oxidation by 0.1 M $Ce(SO_4)_2$ in aqueous H_2SO_4. This observation is consistent with the current–voltage characteristics of these complexes in Figure 4a which show a much smaller catalytic wave with an onset potential that is shifted positively by several hundred millivolts compared with that of the dimer with aqua ligands.

3. Visible-Light-Induced Generation of Oxygen. Visible-light irradiation of a neutral 10-mL phosphate buffer solution containing

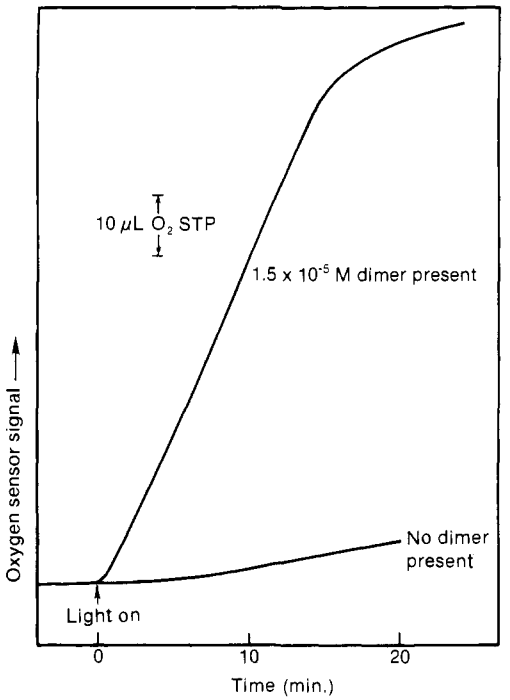

Figure 9. Visible-light-induced oxygen generation in the presence and absence of 1.5×10^{-5} M Ru^{III}–O–Ru^{II} in 10-mL aqueous 0.1 M phosphate buffer, pH 7, at 25 °C with 1×10^{-4} M Ru(II)tris(4,4′-dicarbethoxy-2,2′-bipyridine) as a photosensitizer and 5×10^{-3} M $S_2O_8^{2-}$ as a sacrificial electron acceptor.

1×10^{-4} M Ru(II) tris(4,4′-dicarbethoxy-2,2′-bipyridine) as a photosensitizer (S) and 5×10^{-3} M $S_2O_8^{2-}$ as a sacrificial electron acceptor produces rapid and irreversible bleaching of the dye in the absence of the dimer. In striking contrast, sustained oxygen evolution is observed in the presence of 1.5×10^{-5} M Ru^{III}–O–Ru^{IV}. Figure 9 records these O_2 production results. Oxygen is generated at a rate of 330 μL h^{-1} during the first 15 min. Thereafter, the rate of production declines owing to the gradual depletion of the sensitizer. Spectrophotometric analysis indicated that the dimeric ruthenium complex is not degraded during this reaction. The mechanism for oxygen generation in this system involves photooxidation of the sensitizer by $S_2O_8^{2-}$ followed by water oxidation:[8]

$$2S + S_2O_8^{2-} \xrightarrow{h\nu} 2SO_4^{2-} + 2S^+ \quad (9)$$

$$2S^+ + H_2O \xrightarrow{Ru\text{–}O\text{–}Ru} 2H^+ + 2S + {}^1/_2O_2 \quad (10)$$

Conclusions

The oxo-bridged ruthenium dimer $L_2(H_2O)Ru$–O–$Ru(H_2O)L_2$ has been synthesized and characterized by spectrophotometric and electrochemical techniques. The results show that this dimer is a highly active and durable homogeneous water-oxidation catalyst. The activity of the dimer to catalyze O_2 evolution close to equilibrium conditions is unprecedented for man-made molecular catalysts. Particularly important for development of highly efficient oxygen-evolution catalysts is our finding that introduction of carboxylic acid groups in the 5,5′ positions of the bipyridyl ligands greatly enhances both the catalytic activity and the durability of the dimeric complex. The unsubstituted dimeric complex $(bpy)_2(H_2O)Ru$–O–$Ru(OH_2)(bpy)_2$ is significantly less active and stable than $L_2(H_2O)Ru$–O–$Ru(OH_2)L_2$. The improved characteristics found in $L_2(H_2O)Ru$–O–$Ru(OH_2)L_2$ may be due to a fortunate combination of electronic and steric factors. The elecronic effects introduced by the carboxylic acid groups are revealed in the positive shift of the redox potentials and the red shift of the absorption bands compared to the complex without the carboxylic acid groups.

The present results will greatly facilitate identifying the various oxo-bridged dimers generated during the photolysis and thermolysis of RuL_3^{2+} solutions in the presence of $S_2O_8^{2-}$ in acid medium. Detailed investigation of the mechanism of this reaction, which follows the overall stoichiometry given by eq 5–7, is in progress. In particular, the possibility of forming isomeric dimers with distinct catalytic properties is being scrutinized. It should be noted that the monomer precursor *cis*-$RuL_2(H_2O)_2$ is chiral. Therefore, there exist, apart from the cis and trans configurations, two optical isomers that can combine to give structurally distinct dimers. These structural aspects and their relation to catalytic activity will be addressed in a forthcoming study.

Acknowledgment. The authors are grateful to Dr. Thomas M. Loehr for advice and assistance in acquiring the Raman spectra. This work was supported by the Gas Research Institute (F.P.R., S.M., P.C., and M.G.) and by the Office of Basic Energy Sciences, Division of Chemical Science, U.S. Department of Energy, under Contracts DE-AC02-83CH10093 (F.-J.P. and A.J.F.) and DE-AC06-83ER13111 (J.K.H.).

Registry No. L′, 1762-46-5; RuL'_2Cl_2, 110142-51-3; *cis*-$Ru^{II}L_2Cl_2$, 110173-50-7; *cis*-$Ru^{II}L_2(H_2O)_2^{2+}$, 110142-52-4; $Ru^{II}L_2SO_4$, 110173-51-8; $L_2(H_2O)Ru^{III}$-O-$Ru^{III}(OH_2)L_2Ba$, 110173-52-9; *trans*-$Ru^{II}L_2(H_2O)_2^{2+}$, 110221-05-1; *cis*-$Ru^{III}L_2(H_2O)_2^{3+}$, 110191-19-0; Ru^{III}-O-Ru^{IV}, 110142-53-5; water, 7732-18-5; oxygen, 7782-44-7.